Thematic set:
Carbon forms: paths and processes in the Earth

JGS
Journal of the Geological Society

Published Online First

https://doi.org/10.1144/jgs2018-046

Redox processes and the role of carbon-bearing volatiles from the slab–mantle interface to the mantle wedge

Simone Tumiati[1] & Nadia Malaspina[2]*

[1] Dipartimento di Scienze della Terra, Università degli Studi di Milano, via Mangiagalli 34, 20133 Milano, Italy
[2] Dipartimento di Scienze dell'Ambiente e della Terra, Università degli Studi di Milano Bicocca, Piazza della Scienza 4, 20126 Milano, Italy

N.M., 0000-0002-7089-1035
* Correspondence: nadia.malaspina@unimib.it

Abstract: The valence of carbon is governed by the oxidation state of the host system. The subducted oceanic lithosphere contains considerable amounts of iron so that Fe^{3+}/Fe^{2+} equilibria in mineral assemblages are able to buffer the (intensive) fO_2 and the valence of carbon. Alternatively, carbon itself can be a carrier of (extensive) 'excess oxygen' when transferred from the slab to the mantle, prompting the oxidation of the sub-arc mantle. Therefore, the correct use of intensive and extensive variables to define the slab-to-mantle oxidation by C-bearing fluids is of primary importance when considering different fluid/rock ratios. Fluid-mediated processes at the slab–mantle interface can also be investigated experimentally. The presence of CO_2 (or CH_4 at highly reduced conditions) in aqueous COH fluids in peridotitic systems affects the positions of carbonation or decarbonation reactions and of the solidus. Some methods to produce and analyse COH fluid-saturated experiments in model systems are introduced, together with the measurement of experimental COH fluids composition in terms of volatiles and dissolved solutes. The role of COH fluids in the stability of hydrous and carbonate minerals is discussed comparing experimental results with thermodynamic models and the message of nature.

Received 21 February 2018; **revised** 21 July 2018; **accepted** 20 August 2018

The investigation of redox processes and the role of volatiles especially at the slab–mantle interface are crucial for depicting the framework of Earth carbon cycling. During the early stages of the Earth's history, the abundances of carbon and other volatiles in the different reservoirs were determined by the coupled evolution of the terrestrial magma ocean and the primitive atmosphere (Hier-Majumder & Hirschmann 2017). Since the Archean, the efficient deep subduction of organic carbon produced by photosynthesis could have promoted carbon burial in the mantle and an increase of atmospheric levels of oxygen through time (Duncan & Dasgupta 2017). In this picture the oxidation state of the mantle, mainly governed by Fe^0 and Fe^{2+}/Fe^{3+} ratios, and its dynamics played a key role in modulating the fO_2 of the Earth's surface, leading to the precipitation of minerals in their oxidized forms such as carbonates (Sverjensky & Lee 2010; Andrault *et al.* 2018).

Carbon at the modern terrestrial surface is largely divided between carbonates and organic deposits, with a total budget of 1×10^{23} g C, corresponding to about 100 ppm in the upper mantle (Porcelli & Pepin 2014). Recent estimates from volcanic degassing suggest that the carbon content in the modern deep mantle is even higher (*c.* 263 ppm; Anderson & Poland 2017; Barry 2017). In fact, the fate of carbonates and organic carbon in modern subduction zones is still largely unconstrained, although recent studies suggest that most of the subducted carbon, in the form of carbonates and organic matter, could be recycled back to the surface (Kelemen & Manning 2015).

In this contribution we aim to introduce some basic principles regarding the importance of the use of intensive and extensive variables to define the 'oxidation transfer' from the slab to the overlying mantle by C-bearing fluids, and the buffering capacity of the mantle in the carbon speciation at subduction zones, both from the natural and experimental point of view.

Slab-to-mantle carbon transport: the message from nature

The slab–mantle interface is a key location where fluid-mediated element transfer and redox processes occur (e.g. Hayes & Waldbauer 2006; Manning *et al.* 2013; Debret & Sverjensky 2017). At pressures up to 3 GPa the slab–mantle interface is composed by the mixing of slab and suprasubduction mantle slices in a metasedimentary or ultramafic matrix, to form mélange zones (Bebout 2007; Konrad-Schmolke *et al.* 2011; Marschall & Schumacher 2012; Bostock 2013; Guillot *et al.* 2015; Bebout & Penniston-Dorland 2016). The key point of this geodynamic environment is the presence of high fluid fluxes, which allow the chemical exchange within the mélange materials forming hydrated and low-viscosity layers atop the subducting plate (Schmidt & Poli 2014, and references therein). A different scenario is proposed at higher pressures and temperatures, where the formation of silicate supercritical liquids from dehydration and/or melting of the subducted oceanic crust and metasediments induce percolation by porous flow processes. This process leads to the formation of several hydrous phases, such as amphibole and phlogopite or, occasionally, forms near-monomineralic metasomatic rocks such as orthopyroxenite or phlogopitite layers, acting as a filter for aqueous fluid percolation in the suprasubduction mantle, close to the slab–mantle interface (Manning 2004; Hermann *et al.* 2006; Malaspina *et al.* 2006; Scambelluri *et al.* 2006; Spandler & Pirard 2013).

As will be discussed below, carbon plays a major role in the initiation of metasomatic-related redox processes at the slab–mantle interface. It may release large 'excess oxygen' during redox–decarbonation reactions, if they occur; also, its speciation in metamorphic fluids may govern fluid-related redox reactions. Carbon may be transported at mantle depth by subduction in different forms and oxidation states. Relevant examples of

carbonate-bearing metasediments equilibrated at HP and UHP are provided by eclogitic rocks from the Italian Alps. In his study of impure marbles from the internal Sesia–Lanzo Zone, Castelli (1991) reported a foliation of calcite and dolomite parallel to the eclogitic foliation developed by phengite, quartz, omphacite, grossular-rich garnet, zoisite and Al-rich titanite equilibrated at $P > 1.5$ GPa and $T \sim 600$°C. Another occurrence, from the Dora–Maira UHP terrane, is represented by impure calcite- and dolomite-bearing marbles from Costa Monforte (Castelli *et al.* 2007; Ferrando *et al.* 2017), which show a foliation dominated by carbonates and partial dissolution of dolomite. The best evidence of the dissolution process promoting the carbon transport at depths is provided by the discovery of fluid inclusions in the metamorphosed seafloor Mn-rich sediments from Lago di Cignana (Zermatt–Saas, Italy), containing bicarbonate and carbonate ions, together with crystals of dolomite, magnesite and diamond (Frezzotti *et al.* 2011). In these occurrences carbon is present ubiquitously as C^{4+} and C^0.

Carbon in its oxidized form is also transported during the subduction of carbonates and elemental carbon in meta-ophiolites equilibrated at HP conditions. One example is provided by the work of Ague & Nicolescu (2014), who reported fluid-mediated decarbonation reactions of metacarbonate layers in contact with serpentinite mélange from the islands of Syros and Tinos (Greece). In these rocks carbonate-rich fluid inclusions occur in HP minerals such as omphacite and glaucophane in altered layers surrounding carbonate veins. Graphite associated with calcite has been detected in the serpentinites of Cogne (Italian Western Alps) (Carbonin *et al.* 2015). These phases formed by seafloor metamorphism of mantle peridotites, triggered by carbon-bearing fluids during an advanced stage of the opening of the Alpine Tethys in the Late Jurassic (Toffolo *et al.* 2017). Also, the interaction between metacarbonate rocks and serpentinized mantle occurring at HP has strong implications for the deep transport of oxidized carbon. As shown by Scambelluri *et al.* (2016), dolomite marbles and serpentinites may react during deserpentinization to form carbonate + olivine hybrid rocks, such as those cropping out in the ophicarbonate unit of the Ligurian Western Alps (Italy). A lower degree of carbonate dissolution in serpentinite-derived fluids at more reducing conditions may lead to precipitation of graphite. One example is shown in the Malaspina outcrop (Alpine Corsica) where the sediments in contact with serpentinites develop a reaction zone of graphitic carbonaceous material in the blueschist facies during the Alpine orogeny (Malvoisin *et al.* 2012; Galvez *et al.* 2013). Similar occurrences have been reported by Vitale Brovarone *et al.* (2017) in samples from the Sesia–Lanzo zone in the Western Alps. In this case the reduction of carbonates in ophicarbonates occurring within serpentinized peridotites induces the precipitation of graphite and the formation of methane- and hydrogen-bearing fluid, preserved as inclusions within the matrix calcite. Finally, nearly pure methane or methane-rich fluid inclusions have been found also in UHP eclogites from Dabie-Shan (Fu *et al.* 2003) and in jadeitite from Myanmar, in the Himalayan border of China (Shi *et al.* 2005).

Direct evidence of the transport of carbon-bearing fluids in the suprasubduction mantle and in the mantle wedge are represented by fluid inclusions in peridotites, which are mostly CO_2 bearing (Andersen & Neumann 2001; Frezzotti & Touret 2014; Seo *et al.* 2016). Rarely, fluid inclusions contain methane (Song *et al.* 2009), suggesting that strongly reduced conditions are not a common feature in the lithospheric mantle. CO_2 has been often detected up to 3000 ppm in melt inclusions in olivine from subduction-related igneous rock. However, it is widely accepted that the concentration of CO_2 in these inclusions is lower than in their source magmas because of the partial degassing before melt entrapping (e.g. Metrich & Wallace 2008).

Oxidation state of a rock system: some principles

The valence state of carbon and its speciation are governed by the oxidation state of the host system; that is, by the equilibria among mineral assemblages containing redox-sensitive major elements (e.g. Fe, Mn). Alternatively, the carbon species in subducted rocks and in the deep fluids may control the oxidation state of the host system by redox reactions during metamorphic reactions and fluid–rock interactions. As an example, the so-called DCDD decarbonation–redox reaction occurring in subducted metacarbonates, where dolomite reacts with silica to form diopside, carbon and oxygen, has long been considered one of the redox equilibra at the most oxidizing conditions at which diamond can form in eclogites (Luth 1993):

$$[\text{dolomite}]\ CaMg(CO_3)_2 + [\text{coesite}]\ 2SiO_2 = [\text{diopside}]\ CaMgSi_2O_6 + [\text{diamond}]\ 2C + 2O_2. \quad (1)$$

A dilemma arises about whether the rock system buffers the redox state of carbon or the carbonate-involved redox reactions define the redox state of the rock. To solve this dilemma one must consider (1) the definition of 'oxidation state (or redox state) of a rock' (host system) and the proper use of intensive and extensive variables, (2) the role of 'perfectly mobile and inert components' and (3) the degree of fluid–rock interaction at the slab–mantle interface controlling the C-bearing mass transfer.

A redox equilibrium is defined as a process characterized by the flow of electrons from the substance being oxidized ('reducing medium') to the substance being reduced ('oxidizing medium'). For instance, ionic iron in aqueous solutions is present in two valence states, related by the redox equilibrium

$$Fe^{3+} + e^- = Fe^{2+}. \quad (2)$$

From left to right we have reduction, from right to left we have oxidation. Because oxygen is the most common electron acceptor in natural systems, in Earth Sciences oxidation and reduction generally mean gain and loss of oxygen, by the exchange with an external medium. To rule this exchange, the variable traditionally considered in Earth Sciences is the oxygen fugacity, fO_2 (bar). Because iron is the fourth most abundant element in the Earth's crust, we use oxygen redox buffers considering reactions involving iron-bearing phases (Frost 1991). In the simple system Fe–O–SiO_2, as a first approximation the amount of oxygen is the variable that predicts whether iron can be found as native state, as Fe^{2+} in silicates or as Fe^{2+} or Fe^{3+} in oxides:

$$[\text{wüstite}]\ FeO = [\text{iron}]Fe^0 + 0.5\ O_2\ (\text{IW buffer}) \quad (3)$$

$$[\text{fayalite}]\ Fe_2SiO_4 = [\text{iron}]\ 2Fe^0 + [\text{quartz}]\ SiO_2 + 2\ O_2\ (\text{QIF buffer}) \quad (4)$$

$$[\text{magnetite}]\ 2\ Fe_3O_4 + [\text{quartz}]\ 3\ SiO_2 = [\text{fayalite}]\ 3\ Fe_2SiO_4 + O_2\ (\text{FMQ buffer}) \quad (5)$$

$$[\text{hematite}]\ 6\ Fe_2O_3 = [\text{magnetite}]\ 4\ Fe_3O_4 + O_2\ (\text{HM buffer}). \quad (6)$$

Because in nature solid phases do not usually display pure end-member compositions, most of the redox reactions (including the equilibria (3)–(6)) are not univariant curves, but become multivariant fields. In particular, the replacement of Fe^{2+} by Mg and Ca, and of Fe^{3+} by Al and Cr in iron silicates stabilizes the above equilibria to higher fO_2 (see fig. 9 of Malaspina *et al.* 2009). Similarly, the addition of Fe and the consequent dolomite/diopside activities <1, shift the DCDD buffer (equilibrium (1)) to higher fO_2

(see fig. 2 of Luth 1993). As already pointed out by Frost (1991), in many rocks it is therefore more appropriate to say that oxygen fugacity is a function of the Fe/Mg ratio (and Ca/Mg) of the rock-forming silicates and carbonates.

Oxidation state of 'dirty' rock systems: playing with components

The oxidizing or reducing capacity of a rock is determined by the amount and oxidation state of redox-sensitive major elements, and also by the composition of solid solutions of the mineral assemblages of the rock (Frost 1991). As a consequence, the fO_2 is probably very inhomogeneous in a subducting slab, reflecting the different bulk chemical–mineralogical compositions of the slab lithologies. An attempt to picture this concept has been made by Cannaò & Malaspina (2018), who showed a very complex and inhomogeneous fO_2 pattern in subduction environments, particularly at the interface between the slab and the overlying mantle. Whereas the subducted oceanic crust records ΔFMQ (= $\log fO_2^{sample} - \log fO_2^{FMQ}$; see equilibrium (5)) between ≤0 and +2.5 up to +4, slices from the slab and from the suprasubduction mantle in the subducted mélange look variously oxidized, from ΔFMQ = −1 to ΔFMQ = +12. In this framework, oxygen fugacity is more probably an intensive variable that is governed by the mineral assemblages in the rock, rather than a variable that is imposed from the environment.

The choice of describing the oxidation state of rock systems in terms of the intensive variables fO_2 (bar) and μO_2, which are linked by the relation

$$\mu O_2 \text{ (J mol}^{-1}) = G^0_{f,T,O_2} + R \times T \times \ln fO_2/f^0O_2 \qquad (7)$$

is entirely valid only if O_2 can be considered a 'perfectly mobile' component (Korzhinskii 1936). In open systems a component is defined as 'perfectly mobile' when, during the exchange between the system (e.g. a mineral) and the external medium (e.g. a fluid), the chemical potentials equalize (i.e. they reach equilibrium) in a short time. A component is 'inert' when its exchange between the system and the external medium is difficult and the chemical potentials do not equalize. In the case of perfectly mobile components, the independent parameter must be the chemical potential (e.g. μO_2), whereas if a component is inert the mass of that component (e.g. nO_2) must be considered as the independent parameter. The O_2 molar quantity nO_2 is the conjugate extensive variable of μO_2, similarly to other couples of intensive and extensive variables such as ($P \times -V$) and ($T \times S$) (see details given by Hillert 2008). As shown in a general example by Tumiati *et al.* (2015), considering the variable nO_2 as molar axis, instead of μO_2, the univariant curve separating a phase A and a phase B leaves room for a di-variant two-phase field (A + B). This difference can be easily seen in Figure 1, where a comparison of the variables μO_2 and nO_2 with T is reported for the simple system Fe–O_2. Considering the intensive variable μO_2 as independent (Fig. 1a), the equilibria between magnetite and hematite (blue curve, equilibrium (6)) and between iron and magnetite (pink curve) are univariant. If the extensive variable nO_2 is considered as independent (Fig. 1b), the univariant curves open to di-variant areas, where the relative proportions between magnetite and hematite and between iron and magnetite (horizontal black lines) are ruled by nO_2. As a consequence, oxygen can be added or subtracted in oxygen buffer assemblages without changing μO_2 (or fO_2). The addition of oxygen to a hematite + magnetite assemblage leads thus to an increase in the abundance of hematite, an increase of Fe^{3+}/Fe_{tot} and an increase of nO_2, without changing fO_2, as long as both minerals are present. The system is therefore buffered at constant fO_2 and μO_2.

In geodynamic settings where a high fluid/rock ratio is expected, such as subduction mélanges, oxygen is probably transported along fractures and veins, possibly through mechanisms of dissolution–reprecipitation of O-enriched oxides and silicates (Tumiati *et al.* 2015), or by advective processes (Marschall & Schumacher 2012; Tumiati *et al.* 2013; Nielsen & Marschall 2017). On the other hand, fluid percolation at low fluid/rock ratios occurs when the metasomatic fluid phases produced at UHP interact with peridotitic rocks at the slab–mantle interface. In such occurrences O_2 cannot be considered a perfectly mobile component, because most of the redox reactions take place between solid oxides and silicates, where O_2 is bonded. On this principle, the amount of inert components (e.g. FeO then forming Fe_2O_3 and vice versa) has a fundamental role and the molar quantity of O_2 must be considered as an independent state variable. This concept is well shown in Figure 2, where the redox state of the slab–mantle interface at UHP is portrayed in terms of intensive fO_2, normalized to the FMQ buffer (Fig. 2a) and of extensive nO_2 (Fig. 2b). Figure 2a shows a patchy inhomogeneous redox state of the slab–mantle interface. In this schematic representation three rock systems are considered: (1) slab eclogite, (2) a Grt + Opx-rich layer forming during the reaction of slab-derived supercritical liquids and (3) a suprasubduction metasomatized mantle peridotite. To quantify the redox budget of these three rock systems in terms of extensive nO_2 (Fig. 2b), we must consider Fe^{3+}-bearing minerals (i.e. garnet and clinopyroxene) and their contribution in terms of excess O_2 with respect to a reference state where only Fe^{2+} is present. This approach has been proposed by Tumiati *et al.* (2015) and applied to natural case studies of HP and UHP slab–mantle interaction by Li *et al.* (2016) and Malaspina *et al.* (2017). In the following section we will report step by step how to play with these components.

From fO_2 to nO_2 in 'dirty' rock systems and the role of carbon in the slab-to-mantle oxidation front

We consider the above three rock systems as composed by:

(1) eclogite = 50 mol% garnet + 50 mol% clinopyroxene;
(2) Grt–Opx-rich layer = 10 mol% garnet (+ 90 mol% orthopyroxene);
(3) metasomatized peridotite = 5 mol% garnet + 5 mol% clinopyroxene (+ 90 mol% of olivine and orthopyroxene).

We consider also the Fe^{3+}-bearing component in garnet as skiagite ($Fe_3^{2+}Fe_2^{3+}Si_3O_{12}$) or andradite ($Ca_3Fe_2^{3+}Si_3O_{12}$) and the Fe^{3+}-bearing component in clinopyroxene as aegirine ($NaFe^{3+}Si_2O_6$) or esseneite ($CaFe^{3+}AlSiO_6$). If O_2 is not regarded as a phase or species but merely as a 'stoichiometric' component expressing Fe^{3+}, it can be made explicit in the skiagite ($(FeO)_{0.59}(SiO_2)_{0.35}(O_2)_{0.06}$), andradite ($(CaO)_{0.35}(FeO)_{0.24}(SiO_2)_{0.35}(O_2)_{0.06}$), aegirine ($(Na_2O)_{0.13}(FeO)_{0.27}(SiO_2)_{0.53}(O_2)_{0.07}$) and esseneite ($(CaO)_{0.27}(FeO)_{0.27}(Al_2O_3)_{0.13}(SiO_2)_{0.27}(O_2)_{0.07}$) formulae, rewritten in terms of barycentric molar fractions of oxides and O_2 (Table 1). This means that 1 mole of pure skiagite or andradite and of pure aegirine or esseneite would produce 0.06 and 0.07 moles of excess nO_2 respectively.

Taking into account the garnet (up to 5 mol% of skiagite) and omphacite (up to 6 mol% of aegirine) composition of a mafic eclogite (Proyer *et al.* 2004), 1 mole of eclogite provides 3.6 mmol of excess O_2; that is, 1 m^3 of eclogite contributes for 200 moles of excess O_2 (Fig. 2b). The same calculation can be done considering andradite and esseneite as Fe^{3+} end-members of garnet and omphacite, respectively. The general result will slightly vary (in the error range) owing to the different molar volumes of these two minerals with respect to skiagite and aegirine. Following the above simple calculation, 1 m^3 of Grt–Opx-rich layer probably occurring at the slab–mantle interface with a garnet composition of up to 1.5 mol% of skiagite (Malaspina *et al.* 2017) would contribute

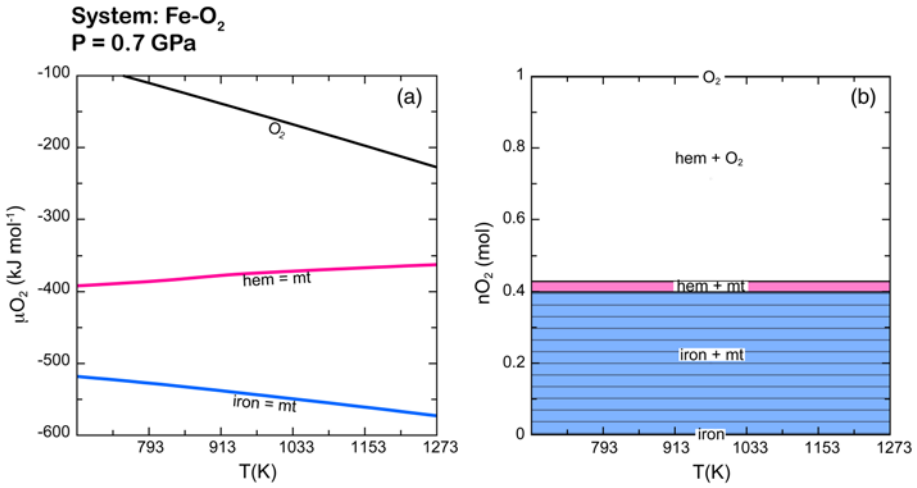

Fig. 1. Comparison between univariant curves and divariant fields in a μO_2 (**a**) and nO_2 (**b**) plot v. *T*, calculated at 0.7 GPa for the system Fe–O_2. Abbreviations: mt, magnetite; hem, hematite.

11 moles of excess O_2; 1 m^3 of suprasubduction metasomatized mantle peridotite such as that from the Chinese Sulu UHP belt, which contains garnet with up to 6 mol% of skiagite and clinopyroxene with up to 5 mol% of aegirine (Malaspina *et al.* 2009, 2012), would contribute 13 moles of excess O_2. As a consequence, as shown in Figure 2, at low fluid/rock ratios mass transfer is supported by a gradient in nO_2 and a metasomatic oxidation front probably develops from the oxidized slab to the overlying mantle. The comparison between Figure 2a and b clearly indicates that the equilibrium attainment is difficult, as the oxygen chemical potentials of these different lithologies do not equalize.

The contribution of excess O_2 owing to reduction of carbonates during the slab-to-mantle metasomatism can be also broadly estimated. As discussed by both thermodynamic and experimental models (e.g. Gorman *et al.* 2006; Poli *et al.* 2009), decarbonation owing to metamorphic reactions is not an efficient mechanism to transfer carbon from the slab to the mantle, because carbonates are stable at *P*–*T* conditions characterizing subduction zones. Let us assume equilibrium (1) as an 'extreme' example of possible redox-induced decarbonation reaction occurring in the slab during subduction. We can use the same approach as described above to model equilibrium (1), making explicit the oxygen produced by reduction of the carbonate ion CO_3^{2-} in dolomite to C (graphite/diamond). One mole of pure dolomite, whose formula can be written as $(CaO)_{0.17}(MgO_2)_{0.17}(C)_{0.33}(O_2)_{0.33}$, would be characterized by 0.33 moles of excess oxygen. Applying equilibrium (1) to a

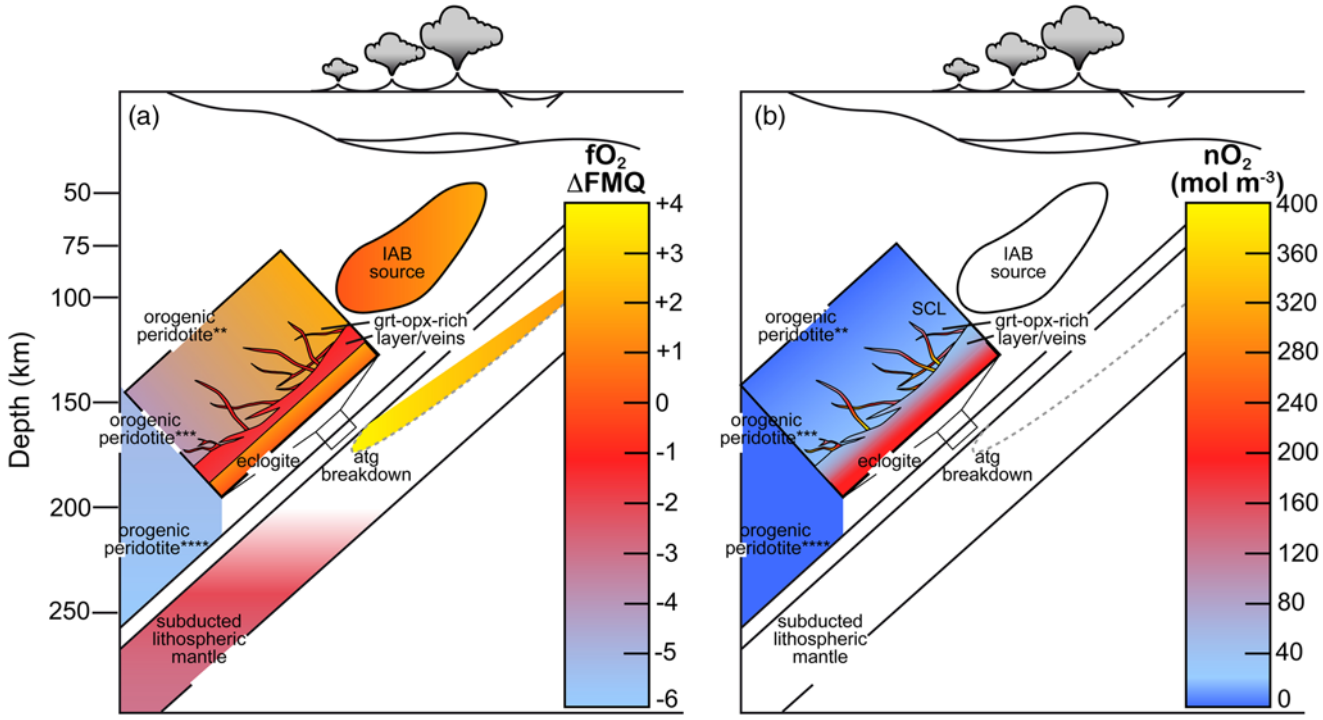

Fig. 2. Schematic illustration showing various redox conditions in terms of intensive ΔFMQ (**a**) and extensive oxygen molar mass (nO_2) (**b**) of subducted lithosphere and suprasubduction mantle at UHP. The colour scale bar is arbitrary, from more reduced rocks (blue) to oxidized rocks (red to yellow). In (**a**), modified after Cannaò & Malaspina (2018), the values of ΔFMQ are from the following literature: eclogite from Mattinson *et al.* (2004), Cao *et al.* (2011) and Li *et al.* (2016); antigorite breakdown from Debret *et al.* (2015); subducted lithospheric mantle from Foley (2010); grt–opx-rich layer or veins from Malaspina *et al.* (2017); orogenic peridotite** from Malaspina *et al.* (2009); orogenic peridotite*** from Malaspina *et al.* (2010) and Rielli *et al.* (2017); orogenic peridotite**** from Rielli *et al.* (2017). For comparison, the oxygen fugacities of island arc basalt (IAB) sources (Ballhaus 1993; Parkinson & Arculus 1999) are also reported. In (**b**) a gradient in nO_2 develops a metasomatic oxidation front from the oxidized slab to the overlying mantle. Atg, antigorite; SCL, supercritical liquids.

Table 1. *Skiagite, andradite, aegirine and esseneite formulae rewritten using O_2 as a component expressing Fe^{3+}*

	Skiagite ($Fe_3^{2+}Fe_2^{3+}Si_3O_{12}$)		Andradite ($Ca_3Fe_2^{3+}Si_3O_{12}$)		Aegirine ($NaFe^{3+}Si_2O_6$)		Esseneite ($CaFe^{3+}AlSiO_6$)	
Components	Moles	NV	Moles	NV	Moles	NV	Moles	NV
SiO_2	3	0.35	3	0.35	2	0.53	1	0.27
FeO	5	0.59	2	0.24	1	0.27	1	0.27
Na_2O	0	0	0	0	0.5	0.13	0	0.00
CaO	0	0	3	0.35	0	0	1	0.27
Al_2O_3	0	0	0	0	0	0	0.5	0.13
O_2	$2 \times 0.25 = 0.5$	0.06	$2 \times 0.25 = 0.5$	0.06	$1 \times 0.25 = 0.25$	0.07	$1 \times 0.25 = 0.25$	0.07
Sum	8.5	1	8.5	1	3.75	1	3.75	1

NV, normalized value. $Fe^{2+} = Fe^{3+} + e^-$. $2\ O^{2-} = O_2 + 4\ e^-$. $0.25\ O^{2-} = 0.25\ O_2 + e^-$.

siliceous dolomitic limestone composed by 40 mol% of dolomite (+ 60 mol% of quartz) (Bucher & Grapes 2011), 1 m^3 of this rock would contribute 6.5×10^4 moles of excess nO_2. This means that if we assume this protolith as a proxy for 1 m^3 of subducted metasediment, the (unlikely) complete reaction would produce a quantity of excess O_2 two orders of magnitude higher compared with that from oceanic subducted rocks, and three orders of magnitude higher compared with that from the suprasubduction mantle wedge. It must be specified that the potential large contribution in excess oxygen of carbonatic metasediments is inhibited by the wide stability of carbonates at oxygen fugacities close to FMQ (Lazar *et al.* 2014), characterizing the slab–mantle interface at sub-arc conditions (Fig. 1). However, natural evidence of carbonate reduction to graphite has been provided in slab rocks at shallower and colder conditions (0.9–1.5 GPa and 430°C; Galvez *et al.* 2013; *c.* 1 GPa and 370°C; Vitale Brovarone *et al.* 2017), where oxygen fugacity conditions close to FMQ are expected to be low enough to reduce carbonates (see below).

Effects of slab-derived COH fluids in the metasomatism of mantle rocks

Although, as discussed above, metamorphic decarbonation is not predicted to be an efficient process at pressures and temperatures typical of subduction zones (see also Kerrick & Connolly 2001; Gorman *et al.* 2006), aqueous dissolution of carbonates (Caciagli & Manning 2003; Pan *et al.* 2013; Ague & Nicolescu 2014; Facq *et al.* 2014) and the upwelling of carbonatitic melts originating from the carbonated oceanic crust (Poli 2015) are considered the most promising vehicles to remobilize carbon towards the mantle wedge, along with diapirism of carbonated subduction mélange (Marschall & Schumacher 2012). The oxidation of organic matter and graphite is another efficient mechanism to produce carbon-rich fluids, especially in the presence of silicate and the consequent decrease in water activity (Tumiati *et al.* 2017), although the total amount of carbon released by this process is poorly constrained owing to the uncertainties associated with the estimated abundance of these phases in subducted rocks (Plank & Langmuir 1998).

The interaction of mantle rocks with carbon-bearing fluids is evidenced by metasomatic assemblages containing carbonates and by carbon-bearing fluid inclusions in mantle minerals. Case studies of slices of metasomatized suprasubduction mantle dragged by the continental crust during subduction and/or exhumation are rare. Among them, we can mention orogenic garnet peridotites and websterites from the Ulten Zone (Italian Alps), Donghai County (Sulu, China) and from Bardane and Ugelvik (Western Gneiss Region, Norway), which experienced metasomatism by ±C-bearing subduction fluid phases up to 200 km depth. Ulten garnet peridotites were metasomatized by slab-derived fluids, which enhanced the crystallization of pargasitic amphibole and dolomite (Sapienza *et al.* 2009; Malaspina & Tumiati 2012; Förster *et al.* 2017). Sulu peridotites record a multistage metasomatism by alkali-rich silicate melt, and a subsequent influx of a slab-derived incompatible element and silicate-rich fluid, which crystallized phlogopite and magnesite during the Triassic UHP metamorphism (Zhang *et al.* 2007; Malaspina *et al.* 2009). Websterites from Bardane preserve remnants of crust-derived fluids, which precipitated graphite/diamond + dolomite/magnesite + Cr-spinel + phlogopite/K-amphibole in multiphase inclusions hosted by majoritic garnet (Van Roermund *et al.* 2002; Scambelluri *et al.* 2008; Malaspina *et al.* 2010). Peridotites from Ugelvik are interlayered with metre-thick lenses of garnet pyroxenites parallel to the compositional banding. These pyroxenites have been described by Carswell (1968, 1973) and interpreted as crystallized at very high temperatures from mantle-derived melts. They are made of porphyroblastic majoritic garnets in equilibrium with clinopyroxene and K-rich amphibole. Bardane websterites and Ugelvik peridotite–clinopyroxenites experienced the prograde subduction at UHP and early retrograde exhumation history of the Baltica plate margin (Spengler *et al.* 2009)

The growth of carbonates in mantle rocks can occur only at relatively low-temperature and high-pressure conditions, above the so-called carbonation surface, represented by the reactions

$$[\text{forsterite}]\ Mg_2SiO_4 + CO_2 = [\text{enstatite}]\ MgSiO_3 + [\text{magnesite}]\ MgCO_3$$

in the Ca-free systems $MS + CO_2$ (Koziol & Newton 1998), and

$$[\text{forsterite}]\ 2Mg_2SiO_4 + [\text{diopside}]\ CaMgSi_2O_6 + 2\ CO_2 = [\text{enstatite}]\ 2Mg_2Si_2O_6 + \text{dolomite}\ CaMg(CO_3)_2 \quad (8)$$

in the Ca-bearing $CMS + CO_2$ (Wyllie *et al.* 1983). Tumiati *et al.* (2013) constrained the dolomite carbonation surface in the more complex hydrous system NKCFMAS + COH at $P > 1.5$ GPa for $T \approx 950$°C, and suggested the following reaction:

$$\text{olivine} + \text{clinopyroxene} + \text{amphibole(I)} + \text{COH fluid} = \text{orthopyroxene} + \text{dolomite} + \text{amphibole(II)} + \text{phlogopite} + \text{garnet} \quad (9)$$

confirming that dolomite is produced at the expense of clinopyroxene and olivine in the mantle wedge metasomatized by CO_2-bearing aqueous fluids.

These reactions are sensitive to the XCO_2 ($= CO_2/(H_2O + CO_2)$) of the fluid phase, as the lower the XCO_2, the higher are the pressures required to accomplish it. Moreover, the position of these reactions in the P–T field varies as a function of the chemical complexity of the thermodynamic system (e.g. Olafsson & Eggler 1983; Wallace & Green 1988). This is consistent, for example, with the occurrence of clinopyroxene-free, dolomite + amphibole peridotites in the Ulten Zone peridotites (Sapienza *et al.* 2009), for which the growth of dolomite in equilibrium with orthopyroxene has been estimated at about 2 GPa and 850°C (Malaspina & Tumiati 2012). In fact, the upper stability of dolomite was defined by Brey

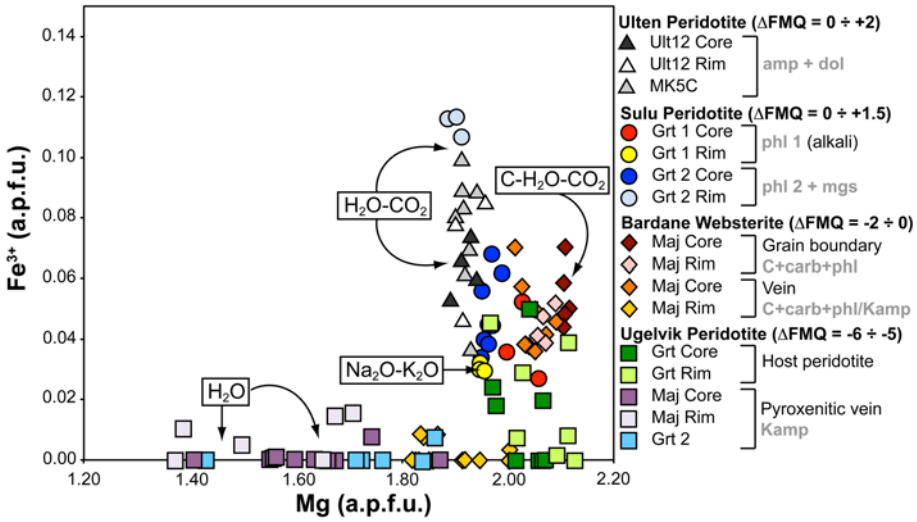

Fig. 3. Ranges of Fe^{3+} contents in garnets from Ulten (Italy), Sulu (China), Bardane and Ugelvik (Norway) peridotites, measured with flank method electron microprobe analyses, plotted v. Mg (atoms per formula unit) as representative of pyrope concentration. Minerals reported to the right of the square brackets indicate the metasomatic hydrous and/or carbonate phases in equilibrium with the analysed garnets. Sources of data: Ulten peridotites from Malaspina *et al.* (2009); Sulu peridotites from Malaspina *et al.* (2009, 2012); Bardane websterites from Malaspina *et al.* (2010); Ugelvik peridotites and clinopyroxenite from Table 2. The decreasing ΔFMQ with increasing pressure equilibration conditions from Ulten to Bardane–Ugelvik peridotites could be biased by the different slopes of the energy surface of the FMQ buffer and that of redox equilibrium between garnet and olivine + orthopyroxene in peridotites (compare Fig. 4).

et al. (1983) in the simple $CaO–MgO–SiO_2$ system by the reaction

$$[\text{enstatite}]\ 2\ MgSiO_3 + [\text{dolomite}]\ CaMg(CO_3)_2 = [\text{diopside}]\ CaMgSi_2O_6 + [\text{magnesite}]\ 2\ MgCO_3 \quad (10)$$

with magnesite being the only stable carbonate ($P > 2.5$ GPa at $T = 900$°C; Tumiati *et al.* 2013).

To relate the oxidation state of metasomatized suprasubduction mantle and the role of COH and alkali components of the crust-

Table 2. *Average major element compositions (wt%) and recalculated formulae of garnets from Ugelvik (Western Gneiss Region, Norway), normalized on the basis of 12 oxygens*

	Host peridotite		Pyroxenite layer			
	Core	Rim	Maj core	Maj rim	Grt_2 core	Grt_2 rim
P (GPa)–*T* (°C):	2–700*		3.5–950†; 3.5–800‡		2–620‡	
No. of analyses:	9	6	16	11	7	5
SiO_2	40.98 (0.34)	41.09 (0.35)	40.82 (0.24)	40.69 (0.31)	40.93 (0.29)	40.66 (0.38)
TiO_2	0.10 (0.11)	0.08 (0.11)	0.07 (0.02)	0.06 (0.02)	0.05 (0.02)	0.04 (0.02)
Al_2O_3	21.79 (1.15)	21.52 (1.04)	23.03 (0.22)	23.06 (0.18)	23.11 (0.17)	23.09 (0.18)
Cr_2O_3	2.53 (1.78)	2.98 (1.56)	0.11 (0.04)	0.11 (0.04)	0.07 (0.03)	0.08 (0.04)
Fe_2O_3	0.23 (0.32)	0.38 (0.36)	0.08 (0.15)	0.17 (0.46)	0.01 (0.04)	0.00 (0.00)
FeO	10.11 (1.56)	9.03 (1.98)	13.72 (0.55)	13.74 (0.63)	14.28 (0.71)	14.83 (0.74)
MgO	18.92 (0.38)	19.30 (0.61)	14.99 (1.49)	14.67 (1.45)	15.07 (1.28)	15.35 (1.26)
MnO	0.47 (0.05)	0.46 (0.08)	0.30 (0.03)	0.29 (0.04)	0.29 (0.02)	0.30 (0.03)
CaO	4.43 (0.75)	4.66 (0.83)	7.05 (1.95)	7.31 (1.88)	6.59 (2.14)	5.83 (2.24)
Total	99.54 (0.46)	99.50 (0.81)	100.16 (0.35)	100.10 (0.53)	100.40 (0.60)	100.19 (0.69)
Si	2.97 (0.01)	2.97 (0.01)	2.98 (0.01)	2.98 (0.01)	2.98 (0.01)	2.97 (0.01)
Ti	0.01 (0.01)	0.00 (0.01)	0.00 (0.00)	0.00 (0.00)	0.00 (0.00)	0.00 (0.00)
Al	1.86 (0.09)	1.83 (0.07)	1.98 (0.01)	1.99 (0.01)	1.99 (0.01)	1.99 (0.01)
Cr	0.15 (0.10)	0.17 (0.09)	0.01 (0.00)	0.01 (0.00)	0.00 (0.00)	0.00 (0.00)
Fe^{3+}	0.01 (0.02)	0.02 (0.02)	0.00 (0.00)	0.00 (0.01)	0.00 (0.00)	0.00 (0.00)
Fe^{2+}	0.61 (0.09)	0.55 (0.12)	0.85 (0.03)	0.84 (0.03)	0.87 (0.04)	0.91 (0.04)
Mg	2.04 (0.04)	2.08 (0.06)	1.63 (0.12)	1.60 (0.12)	1.64 (0.14)	1.67 (0.13)
Mn	0.03 (0.00)	0.03 (0.00)	0.02 (0.00)	0.02 (0.00)	0.02 (0.00)	0.02 (0.00)
Ca	0.34 (0.06)	0.36 (0.07)	0.54 (0.13)	0.58 (0.12)	0.51 (0.17)	0.46 (0.18)
Cation sum	8.01 (0.01)	8.01 (0.01)	8.02 (0.01)	8.02 (0.01)	8.02 (0.01)	8.03 (0.01)
$Fe^{3+}/\Sigma Fe$	0.00 (0.00)	0.01 (0.01)	0.00 (0.00)	0.00 (0.00)	0.00 (0.00)	0.00 (0.00)
$X_{Mg} = Mg/(Mg + Fe^{2+})$	0.77 (0.03)	0.79 (0.04)	0.66 (0.02)	0.65 (0.02)	0.65 (0.01)	0.65 (0.01)

Numbers in parentheses are the standard deviations relative to the number of analyses reported at the top of the table. $Fe^{3+}/\Sigma Fe$, flank method measurements; Maj, majoritic garnet, Grt, second generation recrystallized garnet.
*Stage III of Van Roermund & Drury (1998)
†Carswell 1973
‡Spengler *et al.* 2009

derived metasomatic agents, we report in Table 2 and Figure 3 the Fe^{3+} measurements of garnets and the calculated fO_2 of the above peridotites. An apparent correlation between the composition of the metasomatic agent (C- and alkali-bearing) and the fluid-induced oxidation of the peridotite mineral assemblage probably exists. Where metasomatism was induced by C-free metasomatic fluids, peridotites do not provide evidence of oxidation and garnets have $Fe^{3+}/\Sigma Fe \cong 0$.

The composition of COH fluids in equilibrium with elemental carbon (i.e. graphite, diamond) is, on the other hand, dependent on the redox state of the system and on the *P*–*T* conditions and can be predicted by conventional thermodynamic models, which rely on equations of state that consider molecular species only (e.g. Connolly & Cesare 1993; Zhang & Duan 2009). On the basis of these models, at fixed *P* and *T* aqueous fluids become enriched in CO_2 in oxidized systems, and in CH_4 in reduced systems, passing through intermediate redox conditions where the abundance of dissolved carbon species is minimized and the activity of water is therefore maximized (Fig. 4). The other COH species (CO, hydrocarbons, H_2, free O_2) have been considered only as minor species at conditions relevant to the upper mantle. However, recent more complex thermodynamic models highlighted the importance of charged carbon species, such as carbonate or bicarbonate ions in relatively oxidized systems and organic dissolved compounds (acetates, formates, propionates) in relatively reduced systems (Sverjensky *et al*. 2014; Pan & Galli 2016; Tiraboschi *et al.* 2018).

Whereas the occurrence of carbonate and bicarbonate species has been demonstrated in experiments (Facq *et al.* 2014), in first-principles molecular dynamic simulations (Pan & Galli 2016) and in natural samples (Frezzotti *et al.* 2011), organic compounds have not yet been detected in experimental fluids. Moreover, the presence of small Raman peaks ascribable to aromatic species have been interpreted as quench products (Li 2016).

Redox buffered fluid–rock interaction: the experimental point of view

Experiments on mantle rocks interacting with carbon-bearing slab-derived fluids have been conducted for decades to retrieve phase stability and melting relations in metasomatized bulk compositions (e.g. Olafsson & Eggler 1983; Wallace & Green 1988). Recent experiments focused on the composition of the equilibrated metasomatizing fluid in terms of dissolved volatile and solute species (Tumiati *et al.* 2017; Tiraboschi *et al.* 2018). Challenging issues of these last experiments are related to the difficulty in extracting fluids avoiding back-reactions in the fluid phase during quench. Further complexities are related to the low amount of fluid present in millimetre-sized experimental capsules, and the tendency of water to condense on the tubing systems, preventing quantitative analyses. *In situ* experiments, carried out in hydrothermal anvil cells, could bypass most of these problems, but are to date limited to relatively low temperatures and very simple chemical systems (e.g.

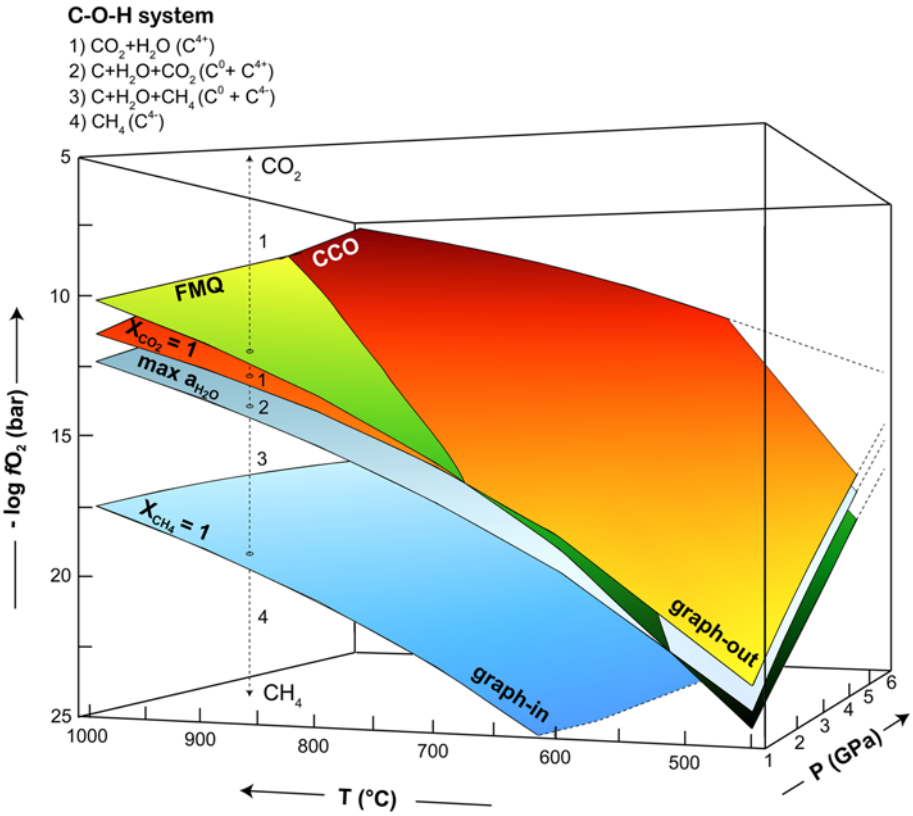

Fig. 4. Three-dimensional diagram for graphite/diamond-saturated COH fluids and compositional isopleths for COH fluids in the *P*–*T*–log fO_2 field. The green surface FMQ indicates the univariant equilibrium (5). XCO_2 and XCH_4 indicate the ratios $CO_2/(H_2O + CO_2)$ and $CH_4/(H_2O + CH_4)$ in the fluid phase, respectively. At $XCO_2 = 1$, carbon polymorphs are in equilibrium with pure CO_2 (CCO). This red-to-yellow surface represents the upper fO_2 stability limit for graphite/diamond in the C–O–H system. At $XCH_4 = 1$, the fluid consists of pure methane. This blue surface represents the lower fO_2 stability limit of graphite/diamond in the C–O–H system. Below this surface, only reduced C^{4-} is stable. The locus of points where the activities of both CO_2 and CH_4 are minimized, and thus the activity of H_2O is maximum, is represented by the light blue surface 'max aH_2O'. Above this surface, CO_2-bearing aqueous fluids are stable, whereas below CH_4 is the dominant carbon species. All calculations were performed using Perple_X (routine 'fluids'; equation [11]) and the COH fluids equation of state of Connolly & Cesare (1993). It should be noted that the FMQ surface is not parallel to the fluid's compositional isopleths, intersecting the CCO surface (i.e. the upper fO_2 stability of elemental carbon described by the reaction $C + O_2 = CO_2$). This means that at low-*P* and high-*T* conditions (e.g. 2 GPa and 900°C) graphite and diamond are not stable at fO_2 = FMQ, because they are fully oxidized to CO_2. On the other hand, at high-*P* and low-*T* conditions (e.g. 5 GPa and 600°C), methane-bearing fluids produced by reduction of graphite/diamond are stable at FMQ conditions.

Facq *et al.* 2014; McCubbin *et al.* 2014). *Ex situ* experiments are more versatile, because a wide range of *P–T–X* conditions can be explored using, for instance, piston cylinders and multi-anvil apparatuses. Moreover, in these experiments the fugacity of oxygen can be controlled using the double-capsule technique (Eugster & Skippen 1967), and the volatiles in the fluid phase quenched to room *T* and *P* (which, however, do not necessarily represent the species in the fluid at the experimental run conditions) can be analysed by mass spectrometry, a technique that provides great sensitiveness to volatile COH species. The first analyses of experimental COH fluids were provided by Eggler *et al.* (1979), who investigated the solubility of CO and CO_2 in various silicate melts at 3 GPa and 1700°C. Recent attempts to measure volatiles in experimental capsules have been described by Dvir *et al.* (2013), who used an IR gas analyser suitable for oxidized H_2O–CO_2 fluids, and by Tiraboschi *et al.* (2016), who used quadrupole mass spectrometry to analyse quantitatively small amount of fluids down to 1 μmol with uncertainties of about 1 mol% for molecular H_2O, CO_2, CO, CH_4, H_2 and O_2. With this technique, Tumiati *et al.* (2017) demonstrated that whereas the composition of COH fluids in equilibrium with graphite at 1–3 GPa and 800°C is consistent with conventional thermodynamic models (Connolly & Cesare 1993; Zhang & Duan 2009), the addition of either quartz or magnesium silicates (forsterite, enstatite) enhances the CO_2 content in high-pressure fluids by 10–30 mol%. In relatively complex systems, therefore, C–O–H models are not fully adequate to predict the composition of slab-derived fluids in terms of dissolved volatiles, and more complex models including dissolved charged species are needed (Sverjensky *et al.* 2014; Galvez *et al.* 2015; Pan & Galli 2016). However, these thermodynamic models still rely on a very limited experimental dataset, so more data on the solubility of minerals in COH fluids would be extremely useful. To date, only few papers have been published on this topic. Newton & Manning (2000) employed the weight-loss technique (Anderson & Burnham 1965) to retrieve the quartz solubility in H_2O–CO_2 fluids, suggesting that it decreases by increasing the CO_2 fraction in the fluid (Newton & Manning 2009). Tumiati *et al.* (2017) and Tiraboschi *et al.* (2018) used a modified version of the so-called cryogenic (or freezing) laser ablation inductively coupled plasma mass spectrometry technique (Kessel *et al.* 2004, 2005) to retrieve the solubility of quartz, forsterite + enstatite and enstatite + magnesite in H_2O–CO_2 fluids in equilibrium with graphite. In contrast to what is observed in graphite-free fluids, the solubility of minerals in the presence of graphite is largely enhanced, presumably because organic Si- and Si–Mg–bearing compounds can form at relatively reduced conditions (Tiraboschi *et al.* 2018).

The fluid phase is therefore somewhat elusive in experiments. In contrast to solid phases, which can be analysed routinely with well-established techniques (e.g. electron microprobe, X-ray diffraction), the analysis of experimental fluids is particularly challenging. Nevertheless, as for any other phase, gaining the composition (and the speciation) of fluids is of fundamental importance and it can be addressed only by combining different experimental approaches and analytical techniques.

Conclusions

The correct use of extensive and intensive parameters in the definition of the redox state of the system depends on whether oxygen can be considered a perfectly mobile component. In natural systems, at low fluid/rock ratios, oxygen is inert and its molar quantity ('excess oxygen' or the 'redox budget' of Evans 2012) must be considered. Alternatively, at high fluid/rock ratios such as in channelized flow regimes and in fluid-saturated experiments, the independent parameter is fO_2. Awareness of this distinction helps to solve the dilemma about whether the valence state of carbon and the speciation of its compounds is governed by the equilibria among mineral assemblages containing redox-sensitive major elements (e.g. Fe, Mn), or the carbon species in subducted rocks and deep fluids control the oxidation state of the host system by redox reactions during fluid–rock interactions.

At redox states fixed by the FMQ buffer, the composition of C-bearing fluids following conventional thermodynamic models is predicted to be a $H_2O + CH_4$ mixture at low *T* and low *P*, nearly pure water at low *T* and high *P*, and $H_2O + CO_2$ at high-*T* conditions. The occurrence of carbon species in different oxidation states may not be directly related to a drastic change in fO_2 (i.e. CH_4 reduced conditions–CO_2 oxidized conditions), but all the variables *P*, *T* and fO_2 must be considered simultaneously. As shown in Figure 4, graphite/diamond-saturated COH fluids can be methane-bearing at FMQ conditions ('oxidized' condition in the mantle) at UHP and relatively low temperature.

Finally, the dissolution of silicates controls the composition of deep COH fluids in equilibrium with graphite, even in the absence of carbonates, boosting the dissolution of graphite in subduction environments at high fluid/rock ratios (mélange) in the form of volatile CO_2.

Acknowledgements We thank R. W. Luth and an anonymous reviewer for their constructive comments. Discussion with S. Poli in the early stage of the paper and the editorial assistance of I. M. Villa significantly helped.

Funding This work was funded by the Deep Carbon Observatory (DCO) and FAR Bicocca: 2015-ATE-0218.

Scientific editing by Igor Villa

References

Ague, J.J. & Nicolescu, S. 2014. Carbon dioxide released from subduction zones by fluid-mediated reactions. *Nature Geoscience*, **7**, 355–360, https://doi.org/10.1038/ngeo2143

Andersen, T. & Neumann, E.-R. 2001. Fluid inclusions in mantle xenoliths. *Lithos*, **55**, 301–320, https://doi.org/10.1016/S0024-4937(00)00049-9

Anderson, G.M. & Burnham, C.W. 1965. The solubility of quartz in supercritical water. *American Journal of Science*, **263**, 494–511.

Anderson, K.R. & Poland, M.P. 2017. Abundant carbon in the mantle beneath Hawaii. *Nature Geoscience*, **10**, https://doi.org/10.1038/NGEO3007

Andrault, D., Muñoz, M. *et al.* 2018. Large oxygen excess in the primitive mantle could be the source of the Great Oxygenation Event. *Geochemical Perspectives Letters*, **6**, 5–10, https://doi.org/10.7185/geochemlet.1801

Ballhaus, C. 1993. Redox states of lithospheric and asthenospheric upper mantle. *Contributions to Mineralogy and Petrology*, **114**, 331–348.

Barry, P.H. 2017. Deep mantle: Enriched carbon source detected. *Nature Geoscience*, **10**, 625–627, https://doi.org/10.1038/ngeo3001

Bebout, G.E. 2007. Metamorphic chemical geodynamics of subduction zones. *Earth and Planetary Science Letters*, **260**, 373–393, https://doi.org/10.1016/j.epsl.2007.05.050

Bebout, G.E. & Penniston-Dorland, S.C. 2016. Fluid and mass transfer at subduction interfaces – The field metamorphic record. *Lithos*, **240–243**, 228–258, https://doi.org/10.1016/j.lithos.2015.10.007

Bostock, M.G. 2013. The Moho in subduction zones. *Tectonophysics*, **609**, 547–557, https://doi.org/10.1016/j.tecto.2012.07.007

Brey, G., Brice, W.R., Ellis, D.J., Green, D.H., Harris, K.L. & Ryabchikov, I.D. 1983. Pyroxene-carbonate reactions in the upper mantle. *Earth and Planetary Science Letters*, **62**, 63–74.

Bucher, K. & Grapes, R. 2011. *Petrogenesis of Metamorphic Rocks*. Springer, Berlin.

Caciagli, N.C. & Manning, C.E. 2003. The solubility of calcite in water at 6–16 kbar and 500–800°C. *Contributions to Mineralogy and Petrology*, **146**, 275–285, https://doi.org/10.1007/s00410-003-0501-y

Cannaò, E. & Malaspina, N. 2018. From oceanic to continental subduction: implications for the geochemical and redox evolution of the supra-subduction mantle. *Geosphere*, **14**, https://doi.org/10.1130/GES01691.1

Cao, Y., Song, S.G., Niu, Y.L., Jung, H. & Jin, Z.M. 2011. Variation of mineral composition, fabric and oxygen fugacity from massive to foliated eclogites during exhumation of subducted ocean crust in the North Qilian suture zone, NW China. *Journal of Metamorphic Geology*, **29**, 699–720.

Carbonin, S., Martin, S., Tumiati, S. & Rossetti, P. 2015. Magnetite from the Cogne serpentinites (Piemonte ophiolite nappe, Italy). Insights into seafloor fluid–rock interaction. *European Journal of Mineralogy*, **27**, 31–50, https://doi.org/10.1127/ejm/2014/0026-2410

Carswell, D.A. 1968. Possible primary upper mantle peridotite in Norwegian basal gneiss. *Lithos*, **1**, 322–355.

Carswell, D.A. 1973. Garnet pyroxenite lens within Ugelvik layered garnet peridotite. *Earth and Planetary Science Letters*, **20**, 347–352.

Castelli, D. 1991. Eclogitic metamorphism in carbonate rocks: the example of impure marbles from the Sesia–Lanzo Zone, Italian Western Alps. *Journal of Metamorphic Geology*, **9**, 61–77, https://doi.org/10.1111/j.1525-1314.1991.tb00504.x

Castelli, D., Rolfo, F., Groppo, C. & Compagnoni, R. 2007. Impure marbles from the UHP Brossasco–Isasca Unit (Dora–Maira Massif, western Alps): Evidence for Alpine equilibration in the diamond stability field and evaluation of the $X(CO_2)$ fluid evolution. *Journal of Metamorphic Geology*, **25**, 587–603, https://doi.org/10.1111/j.1525-1314.2007.00716.x

Connolly, J.A.D. & Cesare, B. 1993. C–O–H–S fluid composition and oxygen fugacity in graphitic metapelites. *Journal of Metamorphic Geology*, **11**, 379–388, https://doi.org/10.1111/j.1525-1314.1993.tb00155.x

Debret, B. & Sverjensky, D.A. 2017. Highly oxidising fluids generated during serpentinite breakdown in subduction zones. *Scientific Reports*, **7**, 10351, https://doi.org/10.1038/s41598-017-09626-y

Debret, B., Bolfan-Casanova, N. *et al.* 2015. Redox state of iron during high-pressure serpentinite dehydration. *Contributions to Mineralogy and Petrology*, **169**, 1–18.

Duncan, M.S. & Dasgupta, R. 2017. Rise of Earth's atmospheric oxygen controlled by efficient subduction of organic carbon. *Nature Geoscience*, **10**, 387–392, https://doi.org/10.1038/ngeo2939

Dvir, O., Angert, A. & Kessel, R. 2013. Determining the composition of C–H–O liquids following high-pressure and high-temperature diamond-trap experiments. *Contributions to Mineralogy and Petrology*, **165**, 593–599, https://doi.org/10.1007/s00410-012-0825-6

Eggler, D., Mysen, B. & Hoering, T. 1979. Gas species in sealed capsules in solid-media, high-pressure apparatus. *Carnegie Institution of Washington Yearbook*, **73**, 228–232.

Eugster, H.P. & Skippen, G.B. 1967. Igneous and metamorphic reactions involving gas equilibria. *In*: Abelson, P.H. (ed.) *Researches in Geochemistry*. Wiley, New York, 450–492.

Evans, K.A. 2012. The redox budget of subduction zones. *Earth-Science Reviews*, **113**, 11–32, https://doi.org/10.1016/j.earscirev.2012.03.003

Facq, S., Daniel, I., Montagnac, G., Cardon, H. & Sverjensky, D.A. 2014. *In situ* Raman study and thermodynamic model of aqueous carbonate speciation in equilibrium with aragonite under subduction zone conditions. *Geochimica et Cosmochimica Acta*, **132**, 375–390, https://doi.org/10.1016/j.gca.2014.01.030

Ferrando, S., Groppo, C., Frezzotti, M.L., Castelli, D. & Proyer, A. 2017. Dissolving dolomite in a stable UHP mineral assemblage: Evidence from Cal–Dol marbles of the Dora–Maira Massif (Italian Western Alps). *American Mineralogist*, **102**, 42–60, https://doi.org/10.2138/am-2017-5761

Foley, S.F. 2010. A reappraisal of redox melting in the Earth's mantle as a function of tectonic setting and time. *Journal of Petrology*, **52**, 1363–1391, https://doi.org/10.1093/petrology/egq061

Förster, B., Braga, R., Aulbach, S., Lo Pò, D., Bargossi, G.M. & Mair, V. 2017. A petrographic study of carbonate phases in the Ulten Zone ultramafic rocks: insights into carbonation in the mantle wedge and exhumation-related decarbonation. *Ofioliti*, **42**, 105–127.

Frezzotti, M. & Touret, J.L.R. 2014. CO_2, carbonate-rich melts, and brines in the mantle. *Geoscience Frontiers*, **5**, 697–710, https://doi.org/10.1016/j.gsf.2014.03.014

Frezzotti, M.L., Selverstone, J., Sharp, Z.D. & Compagnoni, R. 2011. Carbonate dissolution during subduction revealed by diamond-bearing rocks from the Alps. *Nature Geoscience*, **4**, 703–706, https://doi.org/10.1038/ngeo1246

Frost, B.R. 1991. Introduction to oxygen fugacity and its petrologic importance. *In*: Lindsley, D.H. (ed.) *Oxide Minerals: Petrologic and Magnetic Significance*. Mineralogical Society of America, Reviews in Mineralogy, **25**, 1–9.

Fu, B., Touret, J.L.R. & Zheng, Y.F. 2003. Remnants of premetamorphic fluid and oxygen isotopic signatures in eclogites and garnet clinopyroxenite from the Dabie–Sulu terranes, eastern China. *Journal of Metamorphic Geology*, **21**, 561–578, https://doi.org/10.1046/j.1525-1314.2003.00464.x

Galvez, M.E., Beyssac, O., Martinez, I., Benzerara, K., Chaduteau, C., Malvoisin, B. & Malavieille, J. 2013. Graphite formation by carbonate reduction during subduction. *Nature Geoscience*, **6**, 473–477, https://doi.org/10.1038/ngeo1827

Galvez, M., Alexander, J. & Connolly, D. 2015. The solubility of rocks in metamorphic fluids : A model for rock-dominated conditions to upper mantle pressure and temperature. *Earth and Planetary Science Letters*, https://doi.org/10.1016/j.epsl.2015.06.019

Gorman, P.J., Kerrick, D.M. & Connolly, J.A.D. 2006. Modeling open system metamorphic decarbonation of subducting slabs. *Geochemistry, Geophysics, Geosystems*, **7**, https://doi.org/10.1029/2005GC001125

Guillot, S., Schwartz, S., Reynard, B., Agard, P. & Prigent, C. 2015. Tectonic significance of serpentinites. *Tectonophysics*, **646**, 1–19, https://doi.org/10.1016/j.tecto.2015.01.020

Hayes, J.M. & Waldbauer, J.R. 2006. The carbon cycle and associated redox processes through time. *Philosophical Transactions of the Royal Society of London, Series B*, **361**, 931–950, https://doi.org/10.1098/rstb.2006.1840

Hermann, J., Spandler, C., Hack, A. & Korsakov, A. 2006. Aqueous fluids and hydrous melts in high-pressure and ultra-high pressure rocks: Implications for element transfer in subduction zones. *Lithos*, **92**, 399–417, https://doi.org/10.1016/j.lithos.2006.03.055

Hier-Majumder, S. & Hirschmann, M.M. 2017. The origin of volatiles in the Earth's mantle. *Geochemistry, Geophysics, Geosystems*, **18**, 3078–3092, https://doi.org/10.1002/2017GC006937

Hillert, M. 2008. *Phase Equilibria, Phase Diagrams and Phase Transformations*. Cambridge University Press, New York.

Kelemen, P.B. & Manning, C.E. 2015. Reevaluating carbon fluxes in subduction zones, what goes down, mostly comes up. *Proceedings of the National Academy of Sciences of the USA*, **112**, E3997–E4006, https://doi.org/10.1073/pnas.1507889112

Kerrick, D.M. & Connolly, J.A.D. 2001. Metamorphic devolatilization of subducted marine sediments and the transport of volatiles into the Earth's mantle. *Nature*, **411**, 293–296, https://doi.org/10.1038/35077056

Kessel, R., Ulmer, P., Pettke, T., Schmidt, M.W. & Thompson, A.B. 2004. A novel approach to determine high-pressure high-temperature fluid and melt compositions using diamond-trap experiments. *American Mineralogist*, **89**, 1078–1086.

Kessel, R., Schmidt, M.W., Ulmer, P. & Pettke, T. 2005. Trace element signature of subduction-zone fluids, melts and supercritical liquids at 120–180 km depth. *Nature*, **437**, 724–727, https://doi.org/10.1038/nature03971

Konrad-Schmolke, M., O'Brien, P.J. & Zack, T. 2011. Fluid migration above a subducted slab – constraints on amount, pathways and major element mobility from partially overprinted eclogite-facies rocks (Sesia Zone, Western Alps). *Journal of Petrology*, **52**, 457–486, https://doi.org/10.1093/petrology/egq087

Korzhinskii, D.S. 1936. Mobility and inertness of components in metasomatosis. *Akademiya Nauk SSSR, Bulletin Series: Geology*, **I**, 35–60.

Koziol, A.M. & Newton, R.C. 1998. Experimental determination of the reaction: Magnesite + enstatite = forsterite + CO_2 in the ranges 6–25 kbar and 700–1100°C. *American Mineralogist*, **83**, 213–219.

Lazar, C., Zhang, C., Manning, C.E. & Mysen, B.O. 2014. Redox effects on calcite–portlandite–fluid equilibria at forearc conditions: Carbon mobility, methanogenesis, and reduction melting of calcite. *American Mineralogist*, **99**, 1604–1615.

Li, J.L., Gao, J., Klemd, R., John, T. & Wang, X.S. 2016. Redox processes in subducting oceanic crust recorded by sulfide-bearing high-pressure rocks and veins (SW Tianshan, China). *Contributions to Mineralogy and Petrology*, **171**, 72, https://doi.org/10.1007/s00410-016-1284-2

Li, Y. 2016. Immiscible C–H–O fluids formed at subduction zone conditions. *Geochemical Perspectives Letters*, 12–21, https://doi.org/10.7185/geochemlet.1702

Luth, R.W. 1993. Diamonds, eclogites, and the oxidation state of the Earth's mantle. *Science*, **261**, 66–68.

Malaspina, N. & Tumiati, S. 2012. The role of C–O–H and oxygen fugacity in subduction-zone garnet peridotites. *European Journal of Mineralogy*, **24**, 607–618, https://doi.org/10.1127/0935-1221/2012/0024-2213

Malaspina, N., Hermann, J., Scambelluri, M. & Compagnoni, R. 2006. Polyphase inclusions in garnet-orthopyroxenite (Dabie Shan, China) as monitors for metasomatism and fluid-related trace element transfer in subduction zone peridotite. *Earth and Planetary Science Letters*, **249**, 173–187, https://doi.org/10.1016/j.epsl.2006.07.017

Malaspina, N., Poli, S. & Fumagalli, P. 2009. The oxidation state of metasomatized mantle wedge: Insights from C–O–H-bearing garnet peridotite. *Journal of Petrology*, **50**, 1533–1552, https://doi.org/10.1093/petrology/egp040

Malaspina, N., Scambelluri, M., Poli, S., Van Roermund, H.L.M. & Langenhorst, F. 2010. The oxidation state of mantle wedge majoritic garnet websterites metasomatised by C-bearing subduction fluids. *Earth and Planetary Science Letters*, **298**, 417–426, https://doi.org/10.1016/j.epsl.2010.08.022

Malaspina, N., Langenhorst, F., Fumagalli, P., Tumiati, S. & Poli, S. 2012. Fe^{3+} distribution between garnet and pyroxenes in mantle wedge carbonate-bearing garnet peridotites (Sulu, China) and implications for their oxidation state. *Lithos*, **146–147**, 11–17, https://doi.org/10.1016/j.lithos.2012.04.023

Malaspina, N., Langenhorst, F., Tumiati, S., Campione, M., Frezzotti, M.L. & Poli, S. 2017. The redox budget of crust-derived fluid phases at the slab–mantle interface. *Geochimica et Cosmochimica Acta*, **209**, https://doi.org/10.1016/j.gca.2017.04.004

Malvoisin, B., Chopin, C., Brunet, F. & Galvez, M.E. 2012. Low-temperature wollastonite formed by carbonate reduction: a marker of serpentinite redox conditions. *Journal of Petrology*, **53**, 159–176, https://doi.org/10.1093/petrology/egr060

Manning, C.E. 2004. The chemistry of subduction-zone fluids. *Earth and Planetary Science Letters*, **223**, 1–16, https://doi.org/10.1016/j.epsl.2004.04.030

Manning, C.E., Shock, E.L. & Sverjensky, D.A. 2013. The chemistry of carbon in aqueous fluids at crustal and upper-mantle conditions: experimental and theoretical constraints. *In*: Hazen, R.M., Jones, A.P. & Baross, J.A. (eds) *Carbon in Earth*. Mineralogical Society of America and Geochemical Society, Reviews in Mineralogy and Geochemistry, **75**, 109–148.

Marschall, H.R. & Schumacher, J.C. 2012. Arc magmas sourced from mélange diapirs in subduction zones. *Nature Geoscience*, **5**, 862–867, https://doi.org/10.1038/ngeo1634

Mattinson, C.G., Zhang, R.Y., Tsujimori, T. & Liou, J.G. 2004. Epidote-rich talc–kyanite–phengite eclogites, Sulu terrane, eastern China: *PT–f*O_2 estimates and the significance of the epidote–talc assemblage in eclogite. *American Mineralogist*, **89**, 1772–1783.

McCubbin, F.M., Sverjensky, D.A., Steele, A. & Mysen, B.O. 2014. *In-situ* characterization of oxalic acid breakdown at elevated *P* and *T*: Implications for organic C–O–H fluid sources in petrologic experiments. *American Mineralogist*, **99**, 2258–2271, https://doi.org/10.2138/am-2014-4947

Metrich, N. & Wallace, P.J. 2008. Volatile abundances in basaltic magmas and their degassing paths tracked by melt inclusions. *In*: Putirka, K.D. & Tepley, F.J., III (eds) *Minerals, Inclusions and Volcnanic Processes*. Mineralogical Society of America and Geochemical Society, Reviews in Mineralogy and Geochemistry, **69**, 363–402, https://doi.org/10.2138/rmg.2008.69.10

Newton, R.C. & Manning, C.E. 2000. Quartz solubility in H_2O–NaCl and H_2O–CO_2 solutions at deep crust–upper mantle pressures and temperatures: 2–15 kbar and 500–900°C. *Geochimica et Cosmochimica Acta*, **64**, 2993–3005, https://doi.org/10.1016/S0016-7037(00)00402-6

Newton, R.C. & Manning, C.E. 2009. Hydration state and activity of aqueous silica in H_2O–CO_2 fluids at high pressure and temperature. *American Mineralogist*, **94**, 1287–1290, https://doi.org/10.2138/am.2009.3287

Nielsen, S.G. & Marschall, H.R. 2017. Geochemical evidence for mélange melting in global arcs. *Science Advances*, **3**, e1602402, https://doi.org/10.1126/sciadv.1602402

Olafsson, M. & Eggler, D.H. 1983. Phase relations of amphibole, amphibole–carbonate, and phlogopite–carbonate peridotite: petrologic constraints on the asthenosphere. *Earth and Planetary Science Letters*, **64**, 305–315.

Pan, D. & Galli, G. 2016. The fate of carbon dioxide in water-rich fluids under extreme conditions. *Science Advances*, **2**, e1601278, https://doi.org/10.1126/sciadv.1601278

Pan, D., Spanu, L., Harrison, B., Sverjensky, D.A. & Galli, G. 2013. Dielectric properties of water under extreme conditions and transport of carbonates in the deep Earth. *Proceedings of the National Academy of Sciences of the USA*, **110**, 6646–6650, https://doi.org/10.1073/pnas.1221581110

Parkinson, I.J. & Arculus, R.J. 1999. The redox state of subduction zone: insights from arc peridotites. *Chemical Geology*, **160**, 409–423.

Plank, T. & Langmuir, C.H. 1998. The chemical composition of subducting sediment and its consequences for the crust and mantle. *Chemical Geology*, **145**, 325–394, https://doi.org/10.1016/S0009-2541(97)00150-2

Poli, S. 2015. Carbon mobilized at shallow depths in subduction zones by carbonatitic liquids. *Nature Geoscience*, https://doi.org/10.1038/ngeo2464

Poli, S., Franzolin, E., Fumagalli, P. & Crottini, A. 2009. The transport of carbon and hydrogen in subducted oceanic crust: An experimental study to 5 GPa. *Earth and Planetary Science Letters*, **278**, 350–360, https://doi.org/10.1016/j.epsl.2008.12.022

Porcelli, D. & Pepin, R.O. 2014. The origin of noble gases and major volatiles in the terrestrial planets. *In*: Holland, H.D. & Turekian, K.K. (eds) *Treatise on Geochemistry*, 2nd edn. Elsevier, Amsterdam, 383–406, https://doi.org/10.1016/B978-0-08-095975-7.00412-5

Proyer, A., McCammon, C. & Dachs, E. 2004. Pitfalls in geothermobarometry of eclogites: Fe^{3+} and changes in the mineral chemistry of omphacite at ultrahigh pressures. *Contributions to Mineralogy and Petrology*, **147**, 305–318, https://doi.org/10.1007/s00410-004-0554-6

Rielli, A., Tomkins, A.G. *et al.* 2017. Evidence of sub-arc mantle oxidation by sulphur and carbon. *Geochemical Perspectives Letters*, 124–132, https://doi.org/10.7185/geochemlet.1713

Sapienza, G.T., Scambelluri, M. & Braga, R. 2009. Dolomite-bearing orogenic garnet peridotites witness fluid-mediated carbon recycling in a mantle wedge (Ulten Zone, Eastern Alps, Italy). *Contributions to Mineralogy and Petrology*, **158**, 401–420, https://doi.org/10.1007/s00410-009-0389-2

Scambelluri, M., Hermann, J., Morten, L. & Rampone, E. 2006. Melt- v. fluid-induced metasomatism in spinel to garnet wedge peridotites (Ulten Zone, Eastern Italian Alps): clues from trace element and Li abundances. *Contributions to Mineralogy and Petrology*, **151**, 372–394, https://doi.org/10.1007/s00410-006-0064-9

Scambelluri, M., Pettke, T. & van Roermund, H.L.M. 2008. Majoritic garnets monitor deep subduction fluid flow and mantle dynamics. *Geology*, **36**, 59, https://doi.org/10.1130/G24056A.1

Scambelluri, M., Bebout, G.E., Belmonte, D., Gilio, M., Campomenosi, N., Collins, N. & Crispini, L. 2016. Carbonation of subduction-zone serpentinite (high-pressure ophicarbonate; Ligurian Western Alps) and implications for the deep carbon cycling. *Earth and Planetary Science Letters*, **441**, 155–166, https://doi.org/10.1016/j.epsl.2016.02.034

Schmidt, M.W. & Poli, S. 2014. Devolatilization during subduction. *In*: Holland, H.D. & Turekian, K.K. (eds) *Treatise on Geochemistry*, 2nd edn. Elsevier, Amsterdam, 669–701, https://doi.org/10.1016/B978-0-08-095975-7.00321-1

Seo, M., Woo, Y., Park, G., Kim, E., Lim, H.S. & Yang, K. 2016. Mantle-derived CO_2–fluid inclusions in peridotite xenoliths from the alkali basalt, Jeju Island, South Korea. *Journal of the Petrological Society of Korea*, **25**, 39–50, https://doi.org/10.7854/JPSK.2016.25.1.39

Shi, G.U., Tropper, P., Cui, W., Tan, J. & Wang, C. 2005. Methane (CH_4)-bearing fluid inclusions in the Myanmar jadeitite. *Geochemical Journal*, **39**, 503–516, https://doi.org/10.2343/geochemj.39.503

Song, S., Su, L., Niu, Y., Lai, Y. & Zhang, L. 2009. CH_4 inclusions in orogenic harzburgite: Evidence for reduced slab fluids and implication for redox melting in mantle wedge. *Geochimica et Cosmochimica Acta*, **73**, 1737–1754, https://doi.org/10.1016/j.gca.2008.12.008

Spandler, C. & Pirard, C. 2013. Element recycling from subducting slabs to arc crust: A review. *Lithos*, **170–171**, 208–223, https://doi.org/10.1016/j.lithos.2013.02.016

Spengler, D., Brueckner, H.K., Van Roermund, H.L.M., Drury, M.R. & Mason, P.R.D. 2009. Long-lived, cold burial of Baltica to 200 km depth. *Earth and Planetary Science Letters*, **281**, 27–35, https://doi.org/10.1016/j.epsl.2009.02.001

Sverjensky, D.A. & Lee, N. 2010. The Great Oxidation Event and mineral diversification. *Elements*, **6**, 31–36.

Sverjensky, D.A., Stagno, V. & Huang, F. 2014. Important role for organic carbon in subduction-zone fluids in the deep carbon cycle. *Nature Geoscience*, **7**, 909–913, https://doi.org/10.1038/ngeo2291

Tiraboschi, C., Tumiati, S., Recchia, S., Miozzi, F. & Poli, S. 2016. Quantitative analysis of COH fluids synthesized at HP–HT conditions: an optimized methodology to measure volatiles in experimental capsules. *Geofluids*, **16**, 841–855, https://doi.org/10.1111/gfl.12191

Tiraboschi, C., Tumiati, S., Sverjensky, D., Pettke, T., Ulmer, P. & Poli, S. 2018. Experimental determination of magnesia and silica solubilities in graphite-saturated and redox-buffered high-pressure COH fluids in equilibrium with forsterite + enstatite and magnesite + enstatite. *Contributions to Mineralogy and Petrology*, **173**, https://doi.org/10.1007/s00410-017-1427-0

Toffolo, L., Nimis, P., Martin, S., Tumiati, S. & Bach, W. 2017. The Cogne magnetite deposit (Western Alps , Italy): A Late Jurassic seafloor ultramafic-hosted hydrothermal system? *Ore Geology Reviews*, **83**, 103–126, https://doi.org/10.1016/j.oregeorev.2016.11.030

Tumiati, S., Fumagalli, P., Tiraboschi, C. & Poli, S. 2013. An experimental study on COH-bearing peridotite up to 3.2 GPa and implications for crust–mantle recycling. *Journal of Petrology*, **54**, 453–479, https://doi.org/10.1093/petrology/egs074

Tumiati, S., Godard, G., Martin, S., Malaspina, N. & Poli, S. 2015. Ultra-oxidized rocks in subduction mélanges? Decoupling between oxygen fugacity and oxygen availability in a Mn-rich metasomatic environment. *Lithos*, **226**, 116–130, https://doi.org/10.1016/j.lithos.2014.12.008

Tumiati, S., Tiraboschi, C. *et al.* 2017. Silicate dissolution boosts the CO_2 concentrations in subduction fluids. *Nature Communications*, **8**, https://doi.org/10.1038/s41467-017-00562-z

Van Roermund, H.L.M. & Drury, M.R. 1998. Ultra-high pressure ($P > 6$ GPa) garnet peridotites in western Norway: exhumation of mantle rocks from >185 km. *Terra Nova*, **10**, 295–301.

Van Roermund, H.L.M., Carswell, D., Drury, M.R. & Heijboer, T.C. 2002. Microdiamonds in a megacrystic garnet websterite pod from Bardane on the island of Fjørtoft, western Norway: evidence for diamond formation in mantle rocks during deep continental subduction. *Geology*, **30**, 959–962.

Vitale Brovarone, A., Martinez, I., Elmaleh, A., Compagnoni, R., Chaduteau, C., Ferraris, C. & Esteve, I. 2017. Massive production of abiotic methane during subduction evidenced in metamorphosed ophicarbonates from the Italian Alps. *Nature Communications*, **8**, 14134, https://doi.org/10.1038/ncomms14134

Wallace, M.E. & Green, D.H. 1988. An experimental determination of primary carbonatite magma composition. *Nature*, **335**, 343–345.

Wyllie, P.J., Huang, W.-L., Otto, J. & Byrnes, A.P. 1983. Carbonation of peridotites and decarbonation of siliceous dolomites represented in the system CaO–MgO–SiO_2–CO_2 to 30 kbar. *Tectonophysics*, **100**, 359–388, https://doi.org/10.1016/0040-1951(83)90194-4

Zhang, C. & Duan, Z. 2009. A model for C–O–H fluid in the Earth's mantle. *Geochimica et Cosmochimica Acta*, **73**, 2089–2102, https://doi.org/10.1016/j.gca.2009.01.021

Zhang, R.Y., Li, T. *et al.* 2007. Multiple metasomatism in Sulu ultrahigh-*P* garnet peridotite constrained by petrological and geochemical investigations. *Journal of Metamorphic Geology*, **25**, 149–164, https://doi.org/10.1111/j.1525-1314.2006.00683.x